Supplement of Atmos. Meas. Tech., 18, 2463–2479, 2025
https://doi.org/10.5194/amt-18-2463-2025-supplement

Atmospheric Measurement Techniques
Open Access

Supplement of

The UNAM-MARine Aerosol Tank (UNAM-MARAT): an evaluation of the ice-nucleating abilities of seawater from the Gulf of Mexico and the Mexican Pacific

M. Fernanda Córdoba et al.

Correspondence to: Luis A. Ladino (luis.ladino@atmosfera.unam.mx)

Table S1. Coordinates of the sampling sites for the seawater samples for the UNAM-MARAT experiments.

Sampling site	Collection date	Experiment date	Latitude	Longitude
BoA	19/10/21	22/10/21	16°50′37.2″N	99°52′31.1″O
PoV	18/11/21	23/11/21	19°11′13.9″N	96°7′10.8″O
BoSM	09/04/22	10/04/22	19°05′40.0″N	104°21′43″O
		25/04/22		

Methodology for Determining Ice-Active Surface Site Density (n_s)

The approach adopted in this study follows the methodology outlined by Si et al. (2018). Initially, the particle density at a specific relative humidity RH ($\rho_{p,RH}$) was determined using Equation S_E1. Subsequently, the x factor was computed according to Equation S_E2, with particular consideration for marine aerosol particles. Equation S_E3 was employed to calculate n_s, which requires both the particle size distribution measured by the LasAir device and the INP concentrations. The n_s values were determined for each sample (i.e., BoA, PoV, and BoSM), using the respective INP and particle concentrations.

a) Calculation of the particle density at a given RH ($\rho_{p,RH}$)

$$\boldsymbol{\rho}_{\mathrm{p,RH}} = \boldsymbol{\rho}_{\mathrm{w}} + \left(\boldsymbol{\rho}_{\mathrm{p,dry}} - \boldsymbol{\rho}_{\mathrm{w}}\right)\frac{1}{\mathrm{gf}^3} \qquad (\mathbf{S1})$$

where ρ_w is the density of water and $P_{p,dry}$ is the density of the dry particles. 1.87 g cm^{-3} was used for marine aerosol (Si et al., 2018). gf^3 is the hygroscopic growth factor. This factor was obtained from Ming and Russell (2001), using the mean relative humidity of 95%. The aerosol particles were assumed to be composed of 30% of organic species.

b) Calculation of the x factor.

$$\mathbf{x} = \mathbf{gf}\sqrt{\frac{\boldsymbol{\rho}_{\mathrm{p,RH}}}{\chi\boldsymbol{\rho}_0}} \qquad (\mathbf{S2})$$

Where χ the dynamic shape factor for a non-spherical particle shape (1 dimensionless), and ρ_0 the unit density of 1 g cm^{-3}.

c) Calculation of n_s based on the geometric diameters at a given RH.

$$n_{s\_ae\_RH} = \frac{[\mathrm{INP}]}{S_{tot,ae,RH}} = \frac{[\mathrm{INP}]}{\pi x^2 D_{geo,dry}^2 N_{tot}} \qquad (\mathbf{S3})$$

where *[INPs]* is the concentration of INP in L^{-1} for each temperature (i.e., to -20, -25, and -30°C) and each MOUDI stage. $S_{tot,ae,RH}$ is the total surface area based on the aerodynamic diameter at the sampling RH, and N_{tot} is the total number of aerosol particles.

$D_{geo,dry}$ corresponds to the average diameter of each LasAir channel, as shown in Table S2. In this case, it was only taken from 1 to 4 channels since the diameters are slightly comparable with the diameters of the MOUDI stages.

Table S2. Summary of average diameters for each LasAir channel.

LasAir channel	Diameter range (µm)	$D_{geo,dry}$ (µm)	$D_{geo,dry}$ (cm)	$D^2_{geo,dry}$ (cm^2)
D1	0.3 – 0.5	0.4	4.0×10^{-5}	1.60×10^{-9}
D2	0.5 – 1.0	0.75	7.5×10^{-5}	5.62×10^{-9}
D3	1.0 – 5.0	3.0	3.0×10^{-4}	8.99×10^{-8}
D4	5.0 – 10	7.5	7.5×10^{-4}	5.62×10^{-7}

The total number of particles (N_{tot}) were those corresponding to the MOUDI sampling period i.e., ten mins.

It is worth mentioning that when equation S_E3 was applied, the concentration of particles from channel 3 (obtained from the LasAir) was used with the INP concentration found in stages 3, 4, and 5 from de MOUDI.

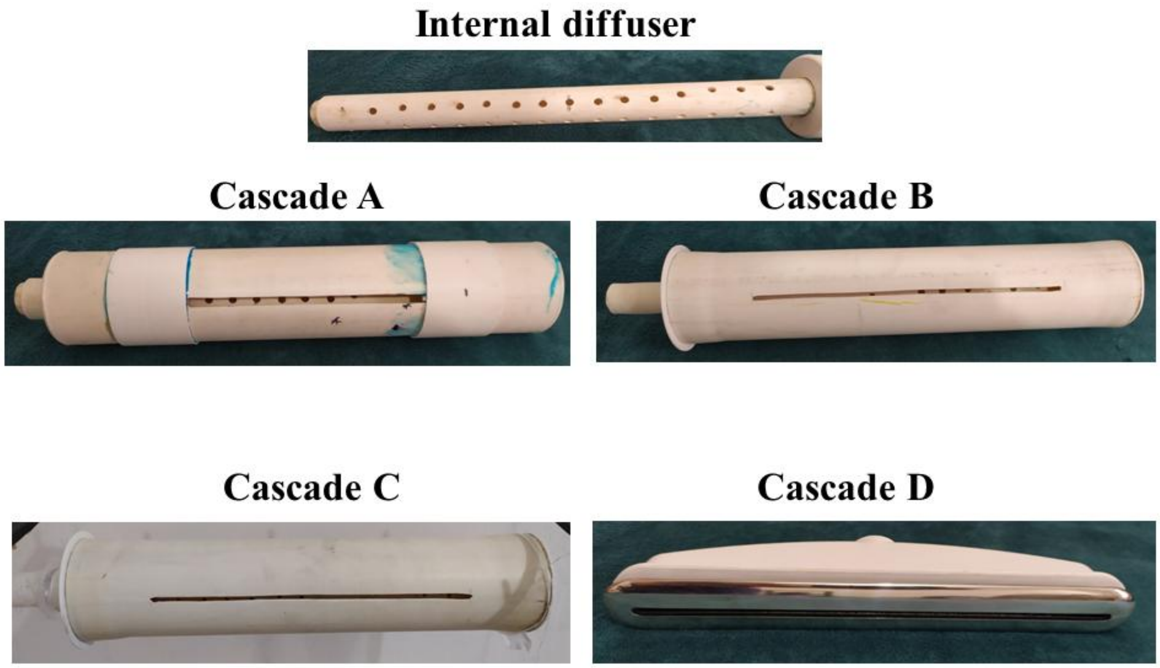

Figure S1. Examples of the homemade and the commercial cascades

Table S3. Characteristics of the cascades evaluated with the UNAM-MARAT.

Cascade	**A**	**B**	**C**	**D**
Number of experiments	12	12	12	12
Length of the slot (cm)	17.5	25.0	25.0	28.3
Width of the slot (mm)	7	4	4	2
Number of holes of the internal diffuser	60	68	68	0
Diameter of the holes of the internal diffuser (mm)	7	7	5	0

Table S4. The n_s and T_{50} values for each sample as a function of particle size.

Sampling site	Variable	T (°C)	Size (µm)						
			10 - 5.6	5.6 - 3.2	3.2- 1.8	1.8 - 1.0	1.0 - 0.56	0.56 - 0.32	0.32- 0.18
BoA	ns (cm^{-2})	-20						388221,9	1817430,1
		-25			785518,3	1961801,6	4052158,8	8618167,6	14101551,1
		-30		906,5	1460405,3	8904128,7	17600641,4	8618167,6	34047932,5
	T_{50} (°C)		-32,0	-27,3	-23,3	-24,0	-25,3	-31,8	-30,3
PoV	ns (cm^{-2})	-20					869,0		
		-25		104,5	447,4	4642,6	4721,6	2300,0	3421,7
		-30		846,3	2873,2	4642,6	4721,6	2300,0	29684,3
	T_{50} (°C)		-30,5	-27,9	-24,0	-23,9	-23,0	-31,6	-31,6
BoSM 09/04/22	ns (cm^{-2})	-20					19,3		
		-25			134,4		281,6	178,3	950,1
		-30		2600,0	578,9		281,6	178,3	950,1
	T_{50} (°C)		-26,6	-23,0	-21,8	-23,5	-27,8	-29,9	-28,8
BoSM 25/04/22	ns (cm^{-2})	-20				24,5	22,4		
		-25			325,0	278,4	182,7	185,0	1253,9
		-30		1698,0	1578,1	278,4	182,7	185,0	1253,9
	T_{50} (°C)		-25,5	-23,5	-22,5	-23,5	-24,1	-25,0	-24,5

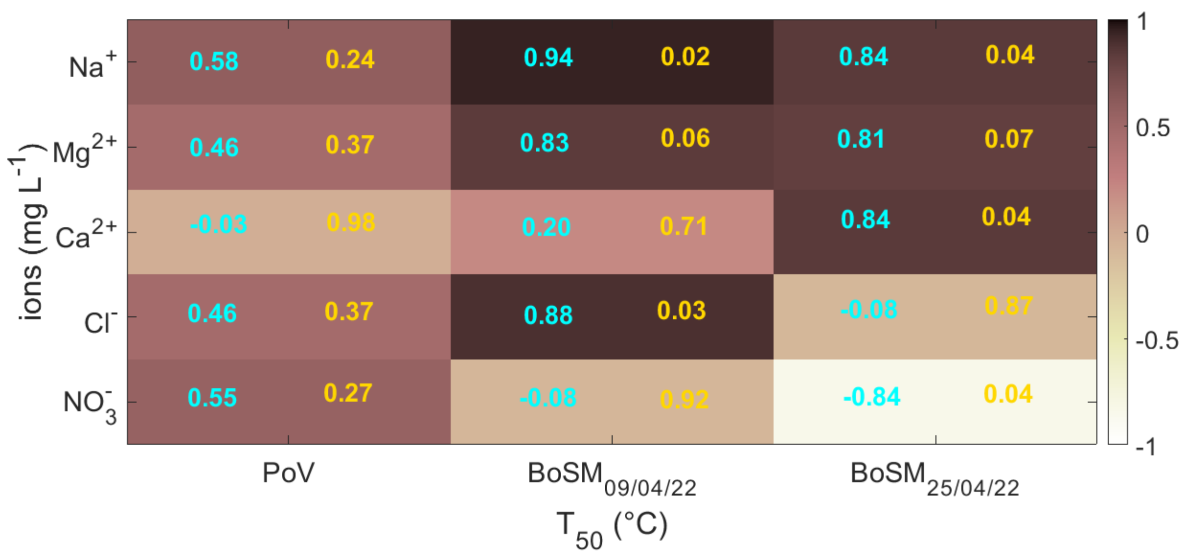

Figure S2. Correlation coefficients (blue numbers) and their respective p-values (yellow numbers, considered significant if $p < 0.05$). Darker and lighter colors indicate a positive and negative correlation, respectively.

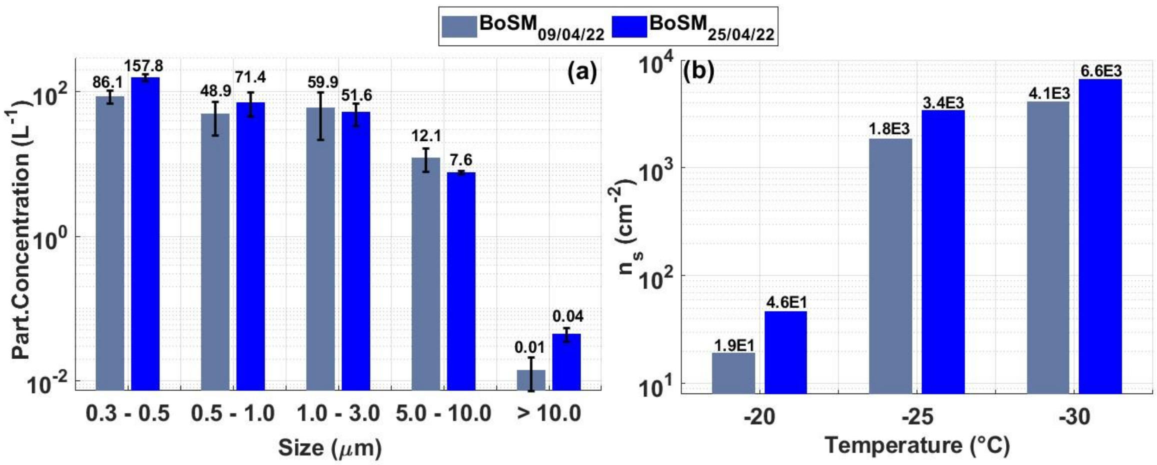

Figure S3. Analysis of transport and aging in the Manzanillo seawater samples (indicate here that 9/April is fresh and grey bars and 25/April is aged sample and blue bars). (a) Particle concentration (L^{-1}) as a function of size (µm) and (b) n_s values as a function of temperature (°C)

References

Ming, Y. and Russell, L. M.: Predicted hygroscopic growth of sea salt aerosol, J. Geophys. Res. Atmos., 106, 28259–28274, https://doi.org/10.1029/2001JD000454, 2001.

Si, M., Irish, V. E., Mason, R. H., Vergara-Temprado, J., Hanna, S. J., Ladino, L. A., Yakobi-Hancock, J. D., Schiller, C. L., Wentzell, J. J. B., Abbatt, J. P. D., Carslaw, K. S., Murray, B. J., and Bertram, A. K.: Ice-nucleating ability of aerosol particles and possible sources at three coastal marine sites, Atmos. Chem. Phys., 18, 15669–15685, https://doi.org/10.5194/acp-18-15669-2018, 2018.